Journal of Computational Applied Mechanics 2023, 54 (1): 49-67

DOI: 10.22059/JCAMECH.2023.353341.788

RESEARCH PAPER

On Numerical Bending Analysis of Functionally Graded Porous Beam – Effect of Porosity Adapting Higher Order Shear Deformation Theory

P. Bridjesh [a,*], G. Chandra Mohana Reddy [a], N.K. Geetha [b], Ch. Ravikiran [a], S. Nagaraju [a]

[a] *Department of Mechanical Engineering, MLR Institute of Technology, Hyderabad, India.*
[b] *Department of Mathematics, Dayananda Sagar College of Engineering, Bengaluru, India*.

Abstract

The bending response of a two- directional functionally graded porous beam (2D-FGPB) is analyzed by adapting a unique shear shape function and taking into consideration even and uneven porosity distributions. Material properties of 2D-FGPB with even and uneven porosity distributions along the length and thickness directions are changed using power law. In formulating equilibrium equations for 2D-FGPB, the principle of virtual displacements is adapted. The method developed by Navier is applied in order to provide solutions to 2D-FGPB for simply supported boundary conditions and is also applied to clamped clamped and clamped free boundary conditions. The proposed methodology is supported by numerical results from published work on non-porous and porous beams. Gradient exponents, porosity, volume fraction, thickness ratio, and aspect ratio have significant influence on the dimensionless transverse deflections and stresses that are studied. The results show that porosity index and aspect ratio play an important role in the bending analysis of the 2D-FGPB

Keywords: *Functionally graded porous beam; Higher order shear deformation theory; Navier's method; Porosity index; Aspect ratio*.

1. Introduction

Functionally graded materials (FGMs) [1] are a type of material that has gradation with variation in microstructure and corresponding changes in characteristics that are being developed and purposefully introduced to improve performance and reliability in either a specific application or within defined functional constraints [2-42]. FGMs microstructures have purposeful spatial non-uniformities. Different material qualities can be combined into one component by considering microstructure as a position-dependent variable [5].

The volume fractions in ceramic and metal regions gradually change in these FGMs' interlayers. Optimized spatial variation in volume fraction reduces thermal pressures that cause the joint to fail during manufacturing or service. FGMs have several uses beyond this, but this is one of the most essential: using material and processing variables, any microstructural trait can be spatially varied [6, 18, 20, 23]. The porous structures are frequently applied in aerospace, marine, and civil engineering. Researchers' interest in functionally graded porous materials has lately increased. FGPMs, where the mechanical properties change constantly along the structure [43]. These are compounds that gradually change in porosity across their volume. The foundation material has a porous structure with a varied

* Bridjesh. Tel.: +91 9849243057; *E-mail address:* meetbridjesh@gmail.com

porosity distribution [19].

Understanding how FGMs react when exposed to static and dynamic loads is essential in structural design. Various theories are proposed to improve predictability of how FGM structures would respond to mechanical loads [21, 44]. Nonlocal elasticity theory and the Gurtin-Murdoch model were used to investigate the vibrational behaviour of a rotating nanobeam [7, 9, 45]. This allowed for the consideration of the effects of interatomic forces as well as the surface energy effect. The differential quadrature approach is utilised in the computation of the nanobeam's vibration frequencies as well as its critical buckling loads [11]. Several researchers have made specific theoretical and experimentally validated theories, such as the strain gradient elasticity theory [4], the higher-order non-local strain gradient theory [10], and the two- layer shear deformation theory [46], to analyse FGMs.

Classical Beam Theory (CBT) was utilised by Wattanasakulpong [47] in their investigation of linear as well as nonlinear vibration in porous beams. The bending and frequency behaviours in porous nano-beams based on CBT were studied by Eltaher et al. [48]. CBT is only applicable to thin beams since it disregards the shear deformation that occurs. Because shear deformation is such an essential factor in beams that are moderate and thick, the First Order Beam Theory (FBT) was created to account for it. Static, buckling, and vibration analyses of porous beams were carried out by Chen et al. [49]. Critical buckling stress and natural frequencies in porous beams strengthened by graphene were predicted in a study by Kitipornchai et al. [50]. Research conducted by Wu et al. [51] looked on the dynamic analysis of beam structures. Gao et al. [52] have developed a computational method for the analysis of the frequencies of beams using FBT. The variations in frequencies in beams were studied by Noori et al. [53], who used the FBT approach in conjunction with the complementary functions method. Lei et al. [54] conducted research to investigate the dynamic analysis of FGB. It is clear that FBT is being used more frequently in the analysis of beams. In order to do so, it requires a shear correction factor that can be tough to ascertain.

Higher Order Beam Theories (HBT) could be considered as a potential solution for FGB. The higher-order nonlocal strain gradient theory [8] was used as the foundation for the development of a novel size dependent plate model. In their analysis, the effects of higher and lower order nonlocalities, as well as the influences of higher-order deformations, were taken into consideration. The revised polynomial [8], trigonometric [55], and exponential shear functions [56] were created for the purpose of performing analysis on beams that were placed on foundations. For the purpose of performing stability and bending calculations on curved beams, Polit et al. [57] presented an HBT. HBT is not required to have a shear correction factor because it uses shear shape functions. Shear shape functions have an important role in the accuracy of HBT. For the purpose of analysing plates made of isotropic material, Shimpi [58] proposed an improved theory wherein, the displacement fields are disintegrated, namely the shear component and the bending component. To analyse FG beams, numerous methods were developed, with the Finite Element Method (FEM) being the one that is used the vast majority of the time. Akbaş [59] proposed a FEM approach for a beam in order to investigate stability and vibration. Analysis of buckling, static and dynamic variations in a curved beam was proposed by Anirudh et al. [60] using a FEM. Fang et al. [61] proposed an iso-geometric analysis method for the static and vibration analysis of thick porous beams. When conducting free vibration analysis on rotating beams, Ebrahimi [62] turned to the differential transform method. Rjoub and Hamad [63] utilized the Transfer Matrix Method to conduct an analysis on vibration of porous beams. In order to study vibration in deep curved beams, Zhao et al. [64] applied a modified version of the Fourier series approach that was derived using the Ritz method. Jamshidi [65] used the Ritz method to study vibration and buckling behaviours in his research on the optimal design of FGB.

This is evident from the fact that the discussions presented above make use of such deformation theories. Because the effect of thickness is vital, particularly for FGBs, the shear and normal deformation theory should be taken into consideration with a variety of boundary conditions, aspect ratios, and gradation exponents. The current theory fulfils zero traction boundary condition on both the top and bottom surfaces of the beam, there is no need for a shear correction factor, which is a factor that depends on the material and geometrical properties as well as the boundary conditions of the FGBs. Higher-order shear deformation theory (HSDT) with nth order can provide accurate structural analysis results.

In this regard, advanced HSDT with nth order is adapted to investigate the bending behaviour of two-directional FGPB that is subjected to different boundary conditions. In combination with analytical solutions and findings from earlier studies, comparative studies are carried out. The numerical calculations are carried out in order to determine the maximum transverse deflections, axial stress, transverse shear stress and normal stress for a different gradation exponent, aspect ratios (L/h), porosity (even and uneven), and sets of boundary conditions such as for simply supported (SS), clamped clamped (CC), and clamped free (CF) beams.

2. Formulation and Mathematics

2.1 Formulation of Porous Functionally Graded Beam

The coordinate system for the beam used in the present research is presented in Figure 1. A rectangular FGB with dimensions of length (L) in x direction, width (b) in y direction, and thickness (h) in z direction. It is assumed that material qualities differ continuously across length and thickness directions. By grading ceramic and metal phases, a FGB in the thickness direction is produced. Here, the lower surface (z = -h/2) is made of metal, and the upper surface (z = +h/2) is made of ceramic. The reference surface, or (z = 0), is the central surface of the beam. Origin (O) is the midpoint of a rectangular beam (x, y), thus z = [-h/2, h/2].

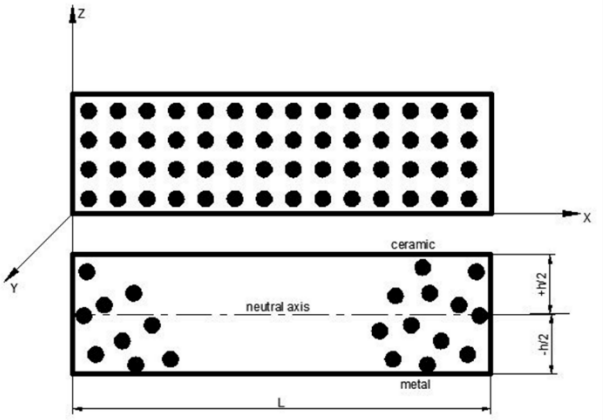

Figure1: functionally graded beam geometry with even and uneven porosity

FGB material properties are determined by the volume proportion of their component materials. It is expected that the thickness coordinate and material characteristics have a functional relationship. The power law distribution in x and z could be used to represent the porous volume fraction (Vf) as shown in Eq. 1 [66].

$$V_f(x,z) = \left(\frac{z}{h}+\frac{1}{2}\right)^{P_z}\left(\frac{x}{L}+\frac{1}{2}\right)^{P_x} \quad (1)$$

where, P_z and P_x denote the behaviour of volume fraction throughout the thickness and length of the beam. The variation of porous volume fractions of ceramic in thickness and length directions is depicted in Figure 2.

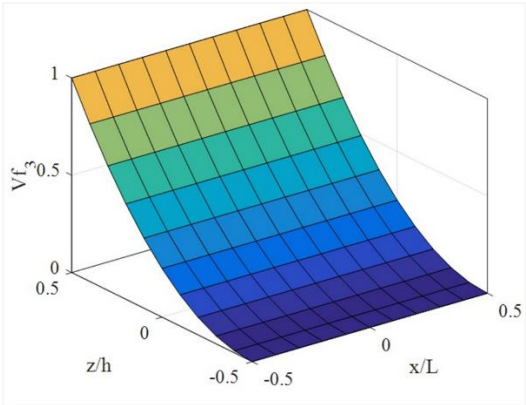

Figure 2: porous volume fraction of ceramic in (z/h) and (x/L) directions

Effective material properties in evenly distributed porous FGB (P) can then be expressed as,

$$P(x,z) = (P_c - P_m)\left(\frac{z}{h}+\frac{1}{2}\right)^{P_z}\left(\frac{x}{L}+\frac{1}{2}\right)^{P_x} + P_m - \frac{\alpha}{2}(P_c + P_m) \quad (2)$$

where α represents the coefficient of porosity ($0 \le \alpha \le 1$), m is metal and c is ceramic. According to the aforementioned relationship, the modulus of elasticity (E) and mass density (ρ) that are used for material stiffness and moment of inertia estimation for evenly distributed 2D-FGPB can be expressed as:

$$E(x,z) = (E_c - E_m)\left(\frac{z}{h}+\frac{1}{2}\right)^{P_z}\left(\frac{x}{L}+\frac{1}{2}\right)^{P_x} + E_m - \frac{\alpha}{2}(E_c + E_m) \quad (2.a)$$

$$\rho(x,z) = (\rho_c - \rho_m)\left(\frac{z}{h}+\frac{1}{2}\right)^{P_z}\left(\frac{x}{L}+\frac{1}{2}\right)^{P_x} + \rho_m - \frac{\alpha}{2}(\rho_c + \rho_m) \quad (2.b)$$

Although a slight variance in Poisson's ratio is seen when compared with other properties, it is considered a constant because computations are made using the average value.

Likewise, the effective properties of material for unevenly distributed 2D-FGPB can then be estimated as,

$$P(x,z) = (P_c - P_m)\left(\frac{z}{h}+\frac{1}{2}\right)^{P_z}\left(\frac{x}{L}+\frac{1}{2}\right)^{P_x} + P_m - \frac{\alpha}{2}(P_c + P_m)\left(1 - \frac{2/z}{h}\right) \quad (3)$$

E and ρ for unevenly distributed 2D-FGPB could be estimated using,

$$E(x,z) = (E_c - E_m)\left(\frac{z}{h}+\frac{1}{2}\right)^{P_z}\left(\frac{x}{L}+\frac{1}{2}\right)^{P_x} + E_m - \frac{\alpha}{2}(E_c + E_m)\left(1 - \frac{2/z}{h}\right) \quad (3.a)$$

and

$$\rho(x,z) = (\rho_c - \rho_m)\left(\frac{z}{h}+\frac{1}{2}\right)^{P_z}\left(\frac{x}{L}+\frac{1}{2}\right)^{P_x} + \rho_m - \frac{\alpha}{2}(\rho_c + \rho_m)\left(1 - \frac{2/z}{h}\right) \quad (3.b)$$

2.2 Constitutive Equations for Displacement Field

To ensure strong construction and lower manufacturing costs, FGBs and plates that experience static and dynamic loads must be well-designed. When analysing FGM structures that are adapted from conventional beam and plate theories, the results of the bending analysis often show that the deflections are underestimated, while the critical loads and natural frequencies are typically overstated. Therefore, it is advised to employ theories that consider shear deformation effects in FGB analysis so as to increase accuracy. Reddy's [10] advanced HSDT is adapted to find the effect of transverse shear and normal strain. The displacement field and constitutive equations are presented as

$$U(x,z,t) = u_0(x,t) + z\emptyset(x,t) - f(z)\left(\emptyset(x,t) + \frac{\partial w_0}{\partial x}(x,t)\right) \quad (4.a)$$

$$W(x,z,t) = w_0(x,t) \quad (4.b)$$

where U and W are axial and transverse displacements, respectively. u_0 and w_0 are axial and transverse displacements at a given point on the neutral axis. $\frac{\partial w_0}{\partial x}$ is the bending slope and $\emptyset$ is shear slope. The displacement field equation in matrix form can be expressed as

$$\binom{U}{W} = \begin{bmatrix}1 & 0 & -z\\ 0 & 1 & 0\end{bmatrix}\{u_0 \quad w_0 \quad w_{0,x}\}^T = [z_d]\{d\} \quad (5)$$

The shear shape function f(z) could be used to determine transverse shear deformation, and the non-zero strain field equations can be computed using Eqs. (4.a) and (4.b) as,

$$\varepsilon_x = \frac{\partial U}{\partial x} = \frac{\partial u_0}{\partial x} - z\frac{\partial^2 w_0}{\partial x^2} + f(z)\left(\frac{\partial \emptyset}{\partial x} + \frac{\partial^2 w_0}{\partial x^2}\right) \quad (6.a)$$

$$\varepsilon_z = \frac{\partial W}{\partial z} = 0 \quad (6.b)$$

$$\gamma_{xz} = f'\left[\emptyset + \frac{\partial w_0}{\partial x}\right] \quad (6.c)$$

$$\text{and } f(z) = \frac{h}{\pi} * sin\left[\frac{\pi * z}{h}\right] - \frac{z}{\pi * n}\left(1 - \frac{1}{n} * \frac{2}{h}^{n-1} * z^{n-1}\right) \quad (7.a)$$

$$f'(z) = \frac{h}{\pi} * sin\left[\frac{\pi}{h}\right] - \frac{1}{\pi * n}\left(1 - \frac{1}{n} * \frac{2}{h}^{n-1} * (n-1)z^{n-2}\right) \quad (7.b)$$

According to Hooke's Law and using Eqs. (6.a), (6.b), (6.c), (7.a), and (7.b), the field equations for stress can be deduced as follows:

$$\sigma_x = \frac{E(x,z)}{1-\mu^2}\varepsilon_x \quad (8.a)$$

and

$$\tau_{xz} = \frac{E(x,z)}{2(1+\mu)}\gamma_{xz} \quad (8.b)$$

2.3 Governing Equations

It is possible to deduce the governing equations by starting with the principle of virtual displacements. The principle that real work can be done virtually in the present can yield

$$\int_0^t (\delta U + \delta V - \delta K)\, dt = 0 \quad (9)$$

where, t denotes time, δU, δV, and δK denotes variations in strain energy, workdone, and kinetic energy, respectively. Variation in strain energy in a 2D-FGPB could be represented as

$$U = \frac{1}{2}\int_0^L \int_{-\frac{h}{2}}^{+\frac{h}{2}} (\sigma_x \varepsilon_x + \tau_{xz}\gamma_{xz}) dz dx \quad (10)$$

$$\delta V = -\int_0^L q\delta w_0\, dx \quad (11)$$

The bending stress of a beam in terms of virtual strain energy and work done can be shown by:

$$B = \delta U + \delta V = 0 \tag{12}$$

$$= \int_0^L \int_{-\frac{h}{2}}^{\frac{h}{2}} (\sigma_x \delta\varepsilon_x + \tau_{xz}\delta\gamma_{xz}) dz dx - \int_0^L q\delta w_0 \, dx = 0 \tag{13}$$

$$= \int_0^L \int_{-h/2}^{h/2} \left(\sigma_x \delta\left(\frac{\partial u_0}{\partial x} - z\frac{\partial^2 w_0}{\partial x^2} + f(z)\left(\frac{\partial \phi}{\partial x} + \frac{\partial^2 w_0}{\partial x^2}\right)\right) + \tau_{xz\delta} f'(z)\left[\emptyset + \frac{\partial w_0}{\partial x}\right]\right) dz dx - \int_0^L q\delta w_0 \, dx = 0 \tag{14}$$

$$= \int_0^L \left(\frac{\partial N_x \delta u_0}{\partial x} - \frac{\partial^2 M_b \delta w_0}{\partial x^2} + \frac{\partial M_s \delta\emptyset}{\partial x} + \frac{\partial^2 M_s \delta w_0}{\partial x^2} + Q_{xz}\delta\emptyset + \frac{\partial Q_{xz}\delta w_0}{\partial x}\right) dx - \int_0^L q\delta w_0 \, dx = 0 \tag{15}$$

$$\begin{bmatrix} N_x \\ M_b \\ M_s \end{bmatrix} = \int_{-\frac{h}{2}}^{\frac{h}{2}} \sigma_x \begin{Bmatrix} 1 \\ z \\ f(z) \end{Bmatrix} dz \tag{16}$$

$$Q_{xz} = \int_{-\frac{h}{2}}^{\frac{h}{2}} \tau_{xz} f'(z) dz \tag{17}$$

where,

N_x is the axial resultant force, M_b is the resultant bending moment, M_s is the resultant moment due to shear deformation, and Q_{xz} is the resultant shear force.

By integrating the displacement gradations, governing equations of equilibrium could be derived.

$$\delta u_0 : \frac{\partial}{\partial x} N_x = 0 \tag{18.a}$$

$$\delta w_0 : \frac{\partial^2}{\partial x^2} M_b - \frac{\partial^2}{\partial x^2} M_x + q - \frac{\partial}{\partial x} Q_{xz} = 0 \tag{18.b}$$

$$\delta\emptyset : \frac{\partial}{\partial x} M_s + Q_{xz} = 0 \tag{18.c}$$

As a result of using Navier's technique, the displacement functions are represented by polynomial series and are shown below, which satisfy the kinematic boundary conditions and are presented in Table 1 [66].

Table 1: various kinematic boundary conditions for numerical computations

Boundary condition	x = -L/2	x = L/2
Simply supported (SS)	u=0, w=0	w=0
Clamped clamped (CC)	u=0, w=0, ϕ=0, w'=0	u=0,w=0, ϕ=0, w'=0
Clamped free (CF)	u=0, w=0, ϕ=0, w'=0	

The coefficients of displacement functions are expressed as

$$u_0(x,t) = \sum_{j=1}^{m} A_j \theta_j(x) e^{i\omega t}, \quad \theta_j(x) = \left(x + \frac{L}{2}\right)^{p_u} \left(x - \frac{L}{2}\right)^{q_u} x^{m-1} \tag{19.a}$$

$$w_0(x,t) = \sum_{j=1}^{m} B_j \varphi_j(x) e^{i\omega t}, \quad \varphi_j(x) = \left(x + \frac{L}{2}\right)^{p_w} \left(x - \frac{L}{2}\right)^{q_w} x^{m-1} \tag{19.b}$$

$$\phi(x,t) = \sum_{j=1}^{m} C_j \psi_j(x) e^{i\omega t}, \quad \psi_j(x) = \left(x + \frac{L}{2}\right)^{p_\phi} \left(x - \frac{L}{2}\right)^{q_\phi} x^{m-1} \tag{19.c}$$

where, u_0, w_0 and ϕ are unknown coefficients, α = πm/ L and ω is the natural frequency of a porous beam. A complex number $i = \sqrt{-1}$ is used to calculate unknown coefficients. A_j, B_j, and C_j. $\theta_j(x)$, $\varphi_j(x)$, and $\psi_j(x)$ are shape functions for boundary conditions. A_j, B_j, and C_j are unknown coefficients that should be estimated. ω is the natural frequency of a beam. p_u, q_u, p_w, q_w, p_ϕ, q_ϕ are the boundary exponents, and the values for boundary exponents can be taken from Table 2 [67].

Table 2: boundary exponents to be used for boundary conditions

Boundary condition	Left end			Right end		
	p_u	p_w	p_ϕ	q_u	q_w	q_ϕ
SS	1	1	0	0	1	0
CC	1	2	1	1	2	1
CF	1	2	1	0	0	0

The transverse load, denoted by q, acts uniformly on the beam's upper surface and is extended using the Fourier series.

$$q = \sum_{m=1,3,5}^{\infty} \frac{4q_0}{m\pi} \, sinax \tag{20}$$

where q_0 is the maximum intensity of load at center of rectangular beam. An analytical solution could be obtained using the following equations by substituting Eqs. (19.a), (19.b), and (19.c) into Eq. (12),

$$S_{11}(i,j) = \frac{E(x,z)}{1-\mu^2}\int_{-\frac{h}{2}}^{\frac{h}{2}} \theta_{i,x}\theta_{j,x}\,dx \quad (21.a)$$

$$S_{12}(i,j) = \frac{E(x,z)}{1-\mu^2}\int_{-\frac{h}{2}}^{\frac{h}{2}} \theta_{i,x}\varphi_{j,xx}\,dx \quad (21.b)$$

$$S_{13}(i,j) = \frac{E(x,z)}{1-\mu^2}\int_{-\frac{h}{2}}^{\frac{h}{2}} \theta_{i,x}\psi_{j,x}\,dx \quad (21.c)$$

$$S_{22}(i,j) = \frac{E(x,z)}{1-\mu^2}\int_{-\frac{h}{2}}^{\frac{h}{2}} \varphi_{i,xx}\varphi_{j,xx}\,dx \quad (21.d)$$

$$S_{23}(i,j) = \frac{E(x,z)}{1-\mu^2}\int_{-\frac{h}{2}}^{\frac{h}{2}} \varphi_{i,xx}\psi_{j,x}\,dx \quad (21.e)$$

$$S_{33}(i,j) = \frac{E(x,z)}{1-\mu^2}\int_{-\frac{h}{2}}^{\frac{h}{2}} \psi_{i,xx}\psi_{j,xx}\,dx \quad (21.f)$$

3. Numerical Computation and Discussion

Numerical results are obtained by using the solutions provided by Navier. The constituents of 2D-FGPB [44] are aluminium metal with a Young modulus of E_m = 70 GPa, Poisson's ratio of μ_m = 0.3, and density of ρ_m = 2702 kg/m^3, and Alumina ceramic with a Young modulus of E_c = 380 GPa, Poisson's ratio of μ_m = 0.3, and density of ρ_c = 3960 kg/m^3. The properties change in thickness as well as length directions, and this variation can be explained by the power law distribution. non-dimensional value indicating the beam's maximum transverse deflection,

$\overline{w} = \frac{100E_m h^3}{q_0 L} w(x,0)$ for SS, CC beams and $\overline{w} = \frac{100E_m h^3}{q_0 L} w(L,0)$ for CF beam. (22)

axial stress (σx), $\overline{\sigma}_x = \frac{\sigma_x h}{q_0 L}$ (23)

and

transverse shear stress (τxz), $\overline{\tau}_{xz} = \frac{\tau_{xz} h}{q_0 L}$ (24)

Adapting the HSDT, an investigation into the static behaviour of 2D-FGPB is carried out. The numerical results for a variety of gradation exponents in both directions (x and z), in addition to a variety of aspect ratios and boundary conditions, could be obtained. The proposed methodology is verified with a simply supported 2D-FGPB that is subjected to uniformly distributed load (UDL). The numerical solutions are evaluated with those obtained from earlier research [66, 68, 69]. In order to make comparisons, transverse deflection, axial stress, shear stress, and normal stress are computed. Tables 3-6 show the comparison of results. It is evident that the outcomes achieved through the use of HSDT are in total agreement with the outcomes of earlier studies.

Table 3. Validation of HSDT with SS boundary conditions in estimating transverse deflection with respect to gradation exponents

Method	Theory	p = 0	p = 1	p = 2	p = 5	p = 10
L/h=5						
[66]	TBT	3.1657	6.2559	8.0602	9.7802	10.8979
[68]	TBT	3.1654	6.2594	8.0677	9.8281	10.9381
[69]	TBT	3.1654	6.2590	8.0668	9.8271	10.9375
Present	HSDT	3.1648	6.2506	8.0535	9.7759	10.8254
L/h=20						
[66]	TBT	2.8962	5.8049	7.4415	8.8151	9.6879
[68]	TBT	2.8962	5.8049	7.4421	8.8182	9.6905
[69]	TBT	2.8963	5.8045	7.4412	8.8173	9.6899
Present	HSDT	2.8845	5.7914	7.4321	8.7958	9.5874

Table 4. Validation of HSDT with SS boundary conditions in estimating axial stress with respect to gradation exponents

Method	Theory	p = 0	p = 1	p = 2	p = 5	p = 10
L/h=5						
[66]	TBT	3.8020	5.8837	6.8812	8.1030	9.7063
[68]	TBT	3.8020	5.8836	6.8826	8.1106	9.7122
[69]	TBT	3.8040	5.8870	6.8860	8.1150	9.7170
Present	HSDT	3.7958	5.8778	6.8719	8.1092	9.6973
L/h=20						
[66]	TBT	15.0130	23.2054	27.0989	31.8112	38.1372
[68]	TBT	15.0129	23.2053	27.0991	31.8130	38.1385
[69]	TBT	15.0200	23.2200	27.1100	31.8300	38.1600
Present	HSDT	15.0132	23.1832	27.1023	31.7812	38.1251

Table 5. Validation of HSDT with SS boundary conditions in estimating transverse shear stress with respect to gradation exponents

Method	Theory	p = 0	p = 1	p = 2	p = 5	p = 10
L/h=5						
[66]	TBT	0.7500	0.7500	0.6787	0.5790	0.6436
[68]	TBT	0.7332	0.7332	0.6706	0.5905	0.6467
[69]	TBT	0.7335	0.7335	0.6700	0.5907	0.6477
Present	HSDT	0.7241	0.7311	0.6854	0.5799	0.6281
L/h=20						
[66]	TBT	0.7500	0.7500	0.6787	0.5790	0.6436
[68]	TBT	0.7451	0.7451	0.6824	0.6023	0.6596
[69]	TBT	0.7470	0.7470	0.6777	0.6039	0.6682
Present	HSDT	0.7581	0.7442	0.6811	0.6102	0.6587s

Table 6. Validation of HSDT with SS boundary conditions in estimating normal shear stress with respect to gradation exponents

Method	Theory	p = 0	p = 1	p = 2	p = 5	p = 10
L/h=5						
[66]	TBT	0.1352	0.0670	0.0925	0.0180	-0.0181
[68]	TBT	0.1352	0.0672	0.0927	0.0182	-0.0179
[69]	TBT	0.1352	0.0671	0.0925	0.0182	-0.0180
Present	HSDT	0.1358	0.0689	0.0925	0.0186	-0.0178
L/h=20						
[66]	TBT	0.0337	-0.5880	-0.6269	-1.1698	-1.5572
[68]	TBT	0.0338	-0.5874	-0.6261	-1.1690	-1.5560
[69]	TBT	0.0338	-0.5880	-0.6226	-1.1760	-1.5589
Present	HSDT	0.0445	-0.6002	0.6311	-1.1971	-1.5436

An analysis is performed on a simply supported 2D-FGPB that is subjected to UDL. Calculations are done to determine transverse deflections and stresses for a number of gradation exponents for different aspect ratios in both directions. Table 7 reveals that there is a negative correlation between aspect ratio and the computed value of transverse deflection. Table 8 presents the dimensionless axial stress. It is obvious that there is a reduction in stress when there is an increase in the gradation exponents in either direction [66]. As presented in Table 9, the highest value of the dimensionless shear stress can be reached when $p_z = 0$ and $p_x = 5$. At an aspect ratio of 20, Table 10 shows that the normal stress nearly disappears.

The effect of porosity on the transverse deflection, axial, shear, and normal stresses is presented in Tables 11 to 14. The variation in transverse deflection, axial, shear, and normal stresses and the effect of porosity (even and uneven) on thickness for different values of the gradation exponent in the x direction are depicted in Figs. 3 - 10 at various aspect ratios. The largest axial stress is found at the beam's upper surface [68].

Table 7. Variation in transverse deflection $\overline{w}$ for SS porous beam with various aspect ratios (L/h = 5, L/h = 20) and gradation exponents

p_z	p_x at L/h = 5				p_x at L/h = 20			
	0	**0.1**	**0.2**	**0.3**	**0**	**0.1**	**0.2**	**0.3**
0	3.667	4.513	5.498	8.795	3.397	4.169	5.071	8.130
1	6.761	7.884	9.015	11.991	6.306	7.329	8.361	11.118
2	8.562	9.591	10.585	13.122	7.943	8.865	9.765	12.112
5	10.282	11.166	12.022	14.172	9.317	10.123	10.914	12.991
10	11.399	12.270	13.085	14.981	10.189	11.022	11.806	13.641

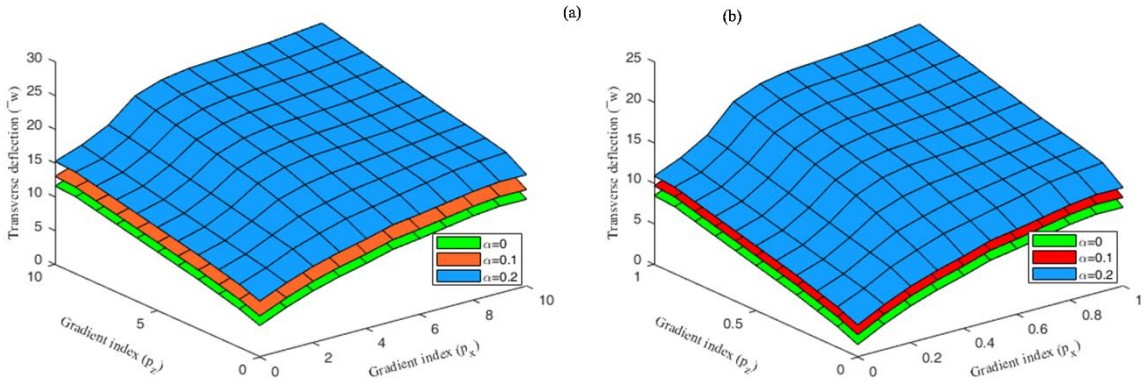

Figure 3: Variation in transverse deflection $\overline{w}$ values of SS beam with various aspect ratios L/h = 5 (a), L/h = 20 (b) and gradation exponents

Table 8. Variation in axial stress $\overline{\sigma}_x$ for SS beam with various aspect ratios (L/h = 5, L/h = 20) and gradation exponents

p_z	p_x at L/h = 5				p_x at L/h = 20			
	0	**0.1**	**0.2**	**0.3**	**0**	**0.1**	**0.2**	**0.3**
0	4.304	4.297	4.272	4.176	15.524	15.498	15.400	15.010
1	6.386	6.200	5.849	5.124	23.707	22.671	21.584	18.712
2	7.383	6.916	6.480	5.448	27.601	25.762	24.041	19.969
5	8.605	7.971	7.385	5.972	32.313	29.845	27.544	22.039
10	10.208	9.342	8.523	6.539	38.639	35.276	32.085	24.479

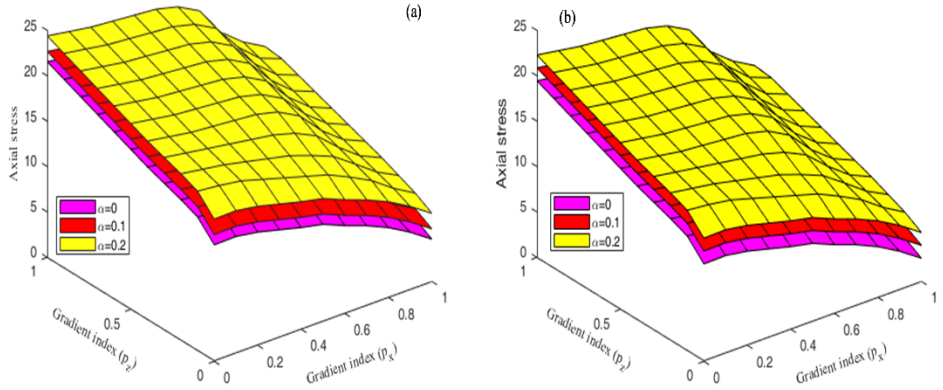

Figure 4. Variation in axial stress $\overline{\sigma}_x$ values of SS beam with various aspect ratios L/h=5 (a), L/h=20 (b) and gradation exponents

Table 9. Variation in shear stress $\overline{\sigma}_{xz}$ values of SS beam with various aspect ratios (L/h = 5, L/h = 20) and gradation exponents

p_z	p_x at L/h = 5				p_x at L/h = 20			
	0	0.1	0.2	0.3	0	0.1	0.2	0.3
0	0.884	0.953	1.009	1.090	0.898	0.969	1.029	1.116
1	0.884	0.939	0.981	1.029	0.898	0.955	0.997	1.046
2	0.820	0.860	0.888	0.918	0.828	0.869	0.898	0.928
5	0.740	0.756	0.766	0.776	0.755	0.774	0.788	0.790
10	0.788	0.794	0.798	0.803	0.820	0.828	0.834	0.833

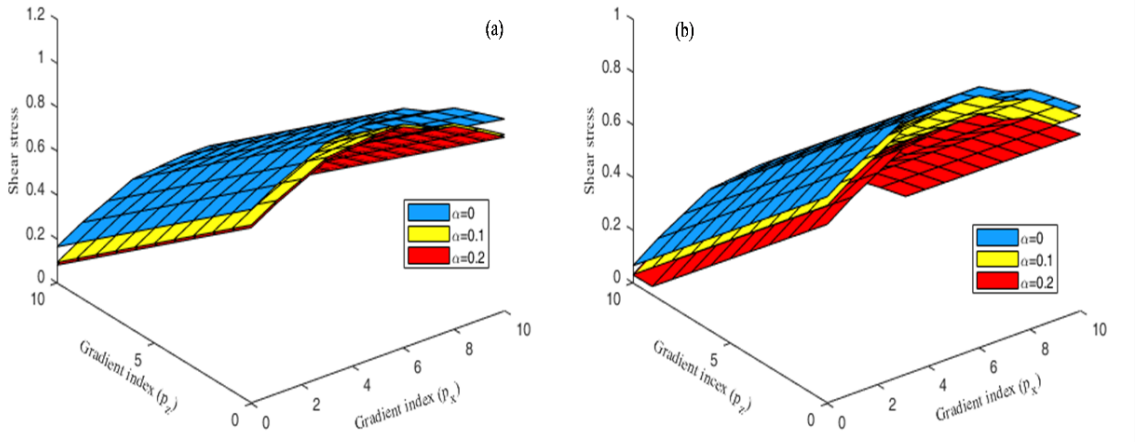

Figure 5. Variation in shear stress $\overline{\sigma}_{xz}$ values of SS beam with various aspect ratios L/h = 5 (a), L/h = 20 (b) and gradation exponents

Table 10: Variation in normal stress $\overline{\sigma}_z$ values of SS beam with various aspect ratios (L/h = 5, L/h = 20) and gradation exponents

p_z	p_x at L/h = 5				p_x at L/h = 20				
	0	**0.1**	**0.2**	**0.3**	**0**	**0.1**	**0.2**	**0.3**	**0**
0	0.1378	0.1375	0.1371	0.1356	0.0342	0.0342	0.0340	0.0336	0.0335
1	0.0693	0.0571	0.0514	0.0656	-0.5885	-0.6020	-0.5869	-0.4232	-0.1164
2	0.0921	0.0580	0.0420	0.0574	-0.6253	-0.7093	-0.7164	-0.5033	-0.1135
5	0.0176	0.0104	0.0198	0.0746	-1.1689	-1.0996	-0.9642	-0.5059	-0.0841
10	-0.0168	0.0146	0.0464	0.1097	-1.5571	-1.2667	-0.9850	-0.3455	-0.0492

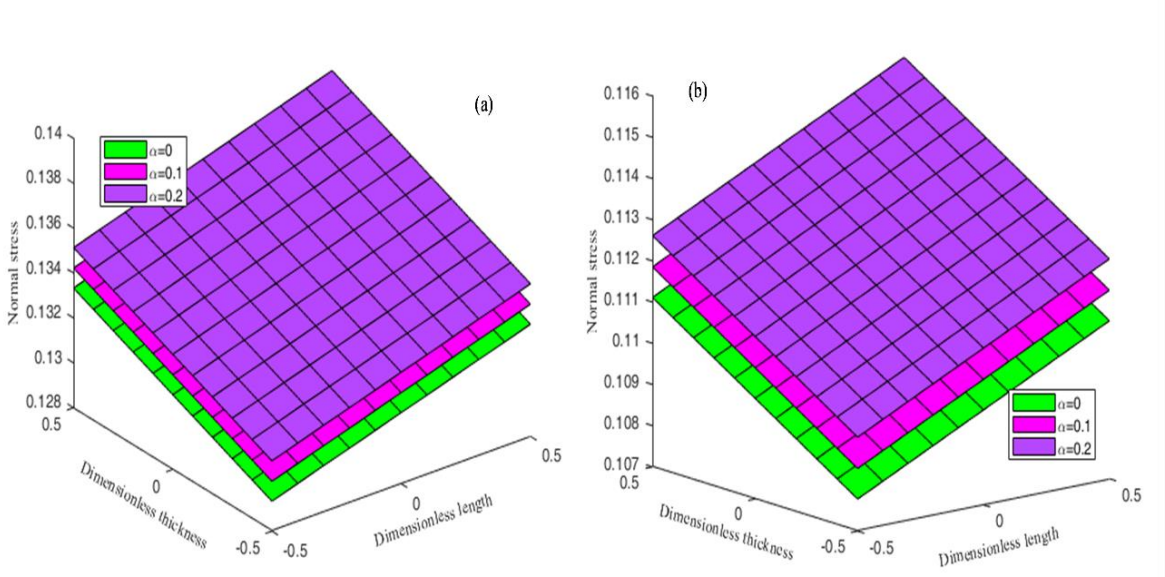

Figure 6. Variation in normal stress $\overline{\sigma}_z$ values of SS beam with various aspect ratios L/h=5 (a), L/h=20 (b) and gradation exponents

Table 11: Variation in transverse deflection $\overline{w}$ values of SS beam with even and uneven porosity, aspect ratio (L/h = 5), and gradation exponents.

p_x & p_z	Even porosity				Uneven porosity			
	0	**0.1**	**0.2**	**0.3**	**0**	**0.1**	**0.2**	**0.3**
0	3.6668	3.9141	4.2039	4.5474	3.6668	3.8385	4.1383	4.4918
1	4.8838	5.3605	5.8605	6.2605	4.8838	5.2849	5.7949	6.2049
2	5.5854	6.8069	7.5171	7.9736	5.5854	6.7313	7.4515	7.9180
5	9.1716	11.146	12.4870	13.113	9.1716	11.071	12.4213	13.0573
10	16.512	18.378	20.7700	21.678	16.512	18.303	20.7043	21.6228

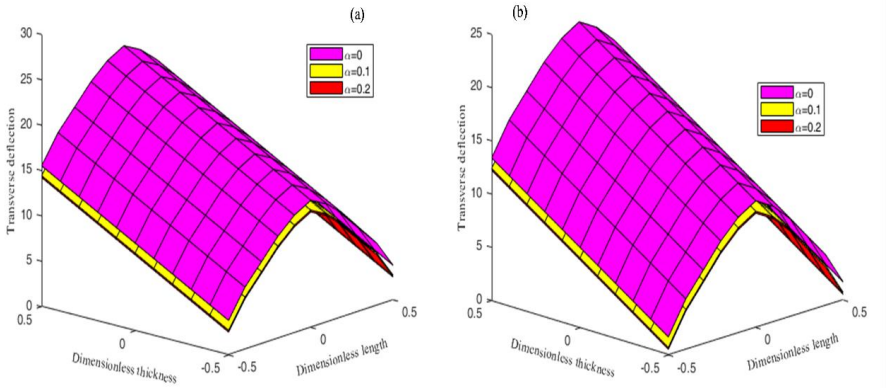

Figure 7. Variation in transverse deflection $\overline{w}$ values of SS beam with even (a) and uneven (b) porosity, aspect ratio (L/h = 5), and gradation exponents

Table 12: Dimensionless axial stress $\overline{\sigma}_x$ values of SS beam with even and uneven porosity, aspect ratio (L/h = 5), and gradation exponents

p_x & p_z	Even porosity				Uneven porosity			
	0	**0.1**	**0.2**	**0.3**	**0**	**0.1**	**0.2**	**0.3**
0	4.3038	4.3008	4.2978	4.2948	4.3038	4.2988	4.2938	4.2888
1	6.1997	6.0331	5.8665	5.6999	6.1997	5.8838	5.5679	5.2520
2	6.4796	6.2836	6.0876	5.8916	6.4796	6.1481	5.8166	5.4851
5	5.9720	5.7882	5.6044	5.4206	5.9720	5.6687	5.3654	5.0621
10	4.8979	4.7322	4.5665	4.4008	4.8979	4.6541	4.4103	4.1665

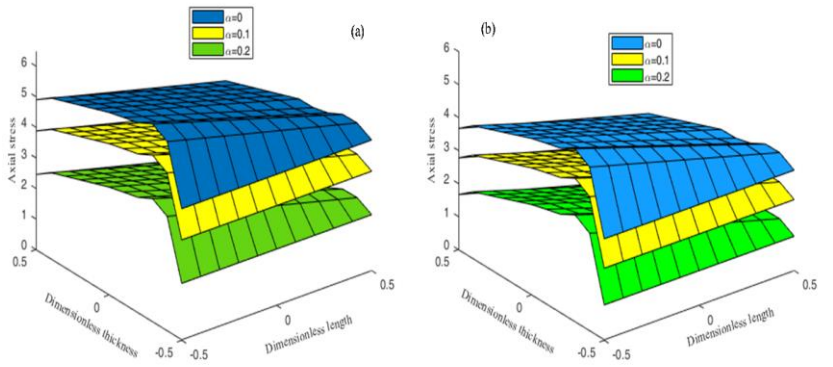

Figure 8. Variation in axial stress $\overline{\sigma}_x$ values of SS beam with even (a) and uneven (b) porosity, aspect ratio (L/h = 5), and gradation exponents

Table 13. Variation in shear stress $\overline{\sigma}_{xz}$ values of SS beam with even and uneven porosity, aspect ratio (L/h = 5), and gradation exponents.

p_x & p_z	Even porosity				Uneven porosity			
	0	**0.1**	**0.2**	**0.3**	**0**	**0.1**	**0.2**	**0.3**
0	0.8101	0.8106	0.8111	0.8119	0.8101	0.7726	0.7267	0.6685
1	0.8122	0.8187	0.8132	0.8144	0.8122	0.7813	0.7446	0.7002
2	0.8205	0.8268	0.8246	0.8286	0.8205	0.7921	0.7590	0.7199
5	0.8387	0.8446	0.8422	0.8599	0.8387	0.8012	0.7723	0.7398
10	0.8215	0.8194	0.8253	0.8310	0.8215	0.7864	0.7580	0.7157

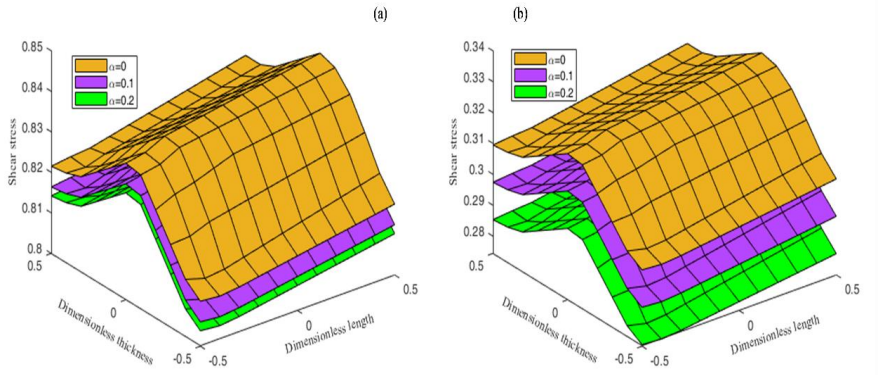

Figure 9. Variation in shear stress $\overline{\sigma}_{xz}$ values of SS beam with even (a) and uneven (b) porosity, aspect ratio (L/h = 5), and gradation exponents

Table 14: Variation in normal stress $\overline{\sigma}_{z}$ values of SS beam with even and uneven porosity, aspect ratio (L/h = 5), and gradation exponents.

p_x & p_z	Even porosity				Uneven porosity			
	0	**0.1**	**0.2**	**0.3**	**0**	**0.1**	**0.2**	**0.3**
0	0.1378	0.1375	0.1368	0.1358	0.1378	0.1281	0.1185	0.1087
1	0.1273	0.0556	0.0502	0.0469	0.1273	0.0530	0.0491	0.0450
2	0.1168	0.0396	0.0377	0.0339	0.1168	0.0530	0.0361	0.0331
5	0.0746	0.0730	0.0704	0.0650	0.0746	0.0693	0.0641	0.0588
10	0.1303	0.1275	0.1229	0.1135	0.1303	0.1211	0.1120	0.1027

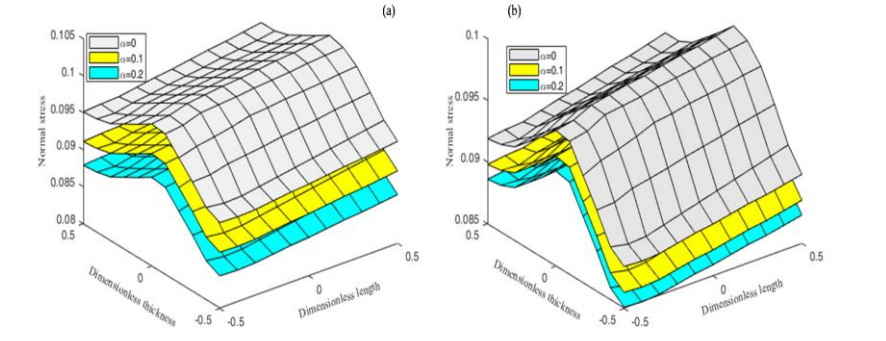

Figure. 10. Variation in normal stress $\overline{\sigma}_{z}$ values of SS beam with even (a) and uneven (b) porosity, aspect ratio (L/h = 5), and gradation exponents

The effect of porosity (even and uneven) is assessed using UDL and various aspect ratios and gradation exponents on SS 2D-FGPB. The aspect ratio decreases the dimensionless transverse deflections. Transverse deflections increase with porosity index (α) in both directions, but even porosity distribution has a higher value than uneven porosity distribution, as shown in Figure 7. Figure 8 shows that dimensionless axial stress decreases with porosity index in both uneven and even distribution, but it is greater in even distribution. The aspect ratio increases the dimensionless shear stress, although gradation exponents reduce it in both directions. The dimensionless shear stress is increased by the porosity index in even distribution but decreased in uneven distribution [42]. Figure 9 shows that uneven porosity distribution reduces the shear stress. Figure 10 shows that, dimensionless normal stress is practically low except at gradation exponent zero in the z-direction. Normal stress decreases with gradation exponent and porosity in both uneven and even distribution, as shown in Figure 10.

Furthermore, the effect of porosity on only CC and CF boundary conditions is presented. Figures 11 to 14 depict the effect of porosity on the transverse deflections of a CC beam. Analysing a CC 2D-FGPB allows for the determination of transverse deflection, axial stress, normal stress, and shear stress while accounting for a variety of aspect ratios and gradation exponents. As the gradation exponent is increased in both directions, the transverse deflection also increases. Nevertheless, the transverse deflection reduces when the aspect ratio is increased. Nevertheless, the greatest value is attained with an even distribution [45], as illustrated in Figure 11. The axial stress of the beam is greatest at its highest point, which is also where the gradation exponent is at its lowest point in z-direction, as depicted in Figure 12. The shear stress value is at its highest point at the centre of the beam Figure 13. The value of normal stress is at its highest point at the top of the beam, as seen in Figure 14.

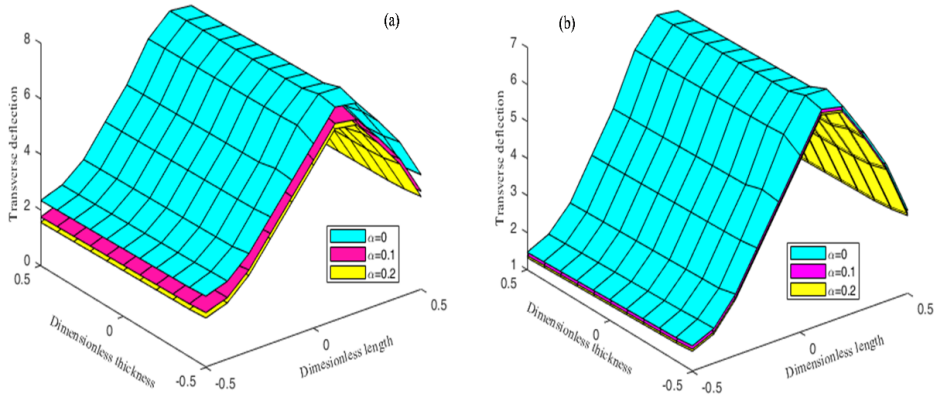

Figure. 11. Variation in transverse deflections $\overline{w}$ values of CC beam with even (a) and uneven (b) porosity, aspect ratio (L/h = 5), and gradation exponents

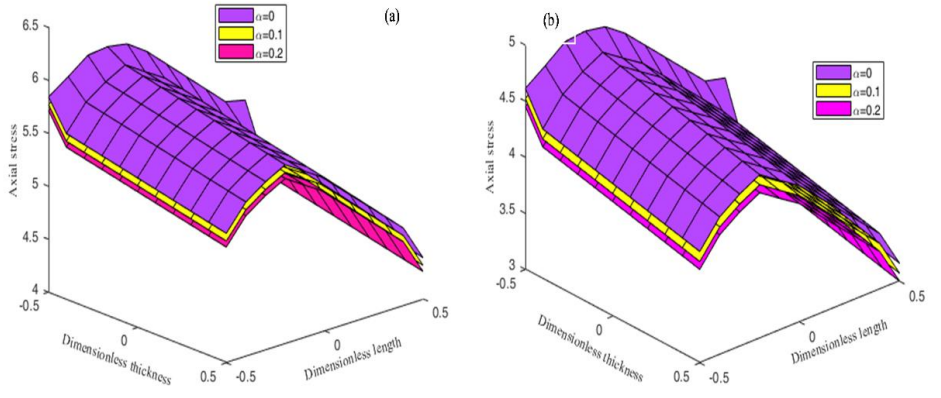

Figure. 12. Variation in axial stress $\overline{\sigma}_x$ values of CC beam with even (a) and uneven (b) porosity, aspect ratio (L/h = 5), and gradation exponents

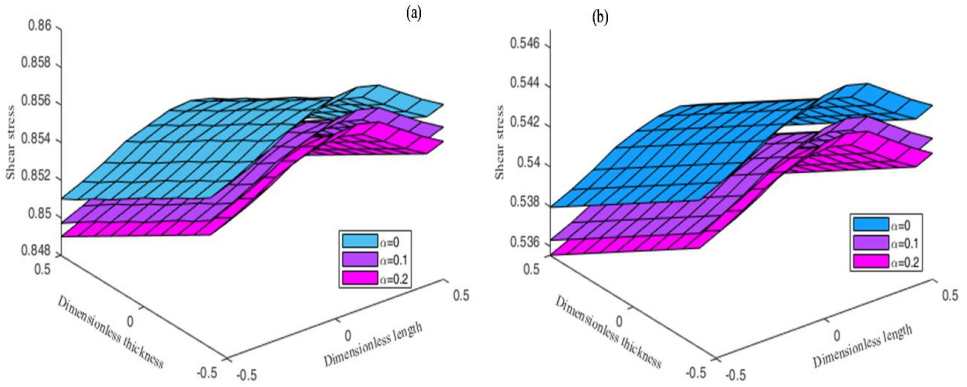

Figure. 13. Variation in shear stress $\overline{\sigma}_{xz}$ values of CC beam with even (a) and uneven (b) porosity, aspect ratio (L/h = 5), and gradation exponents

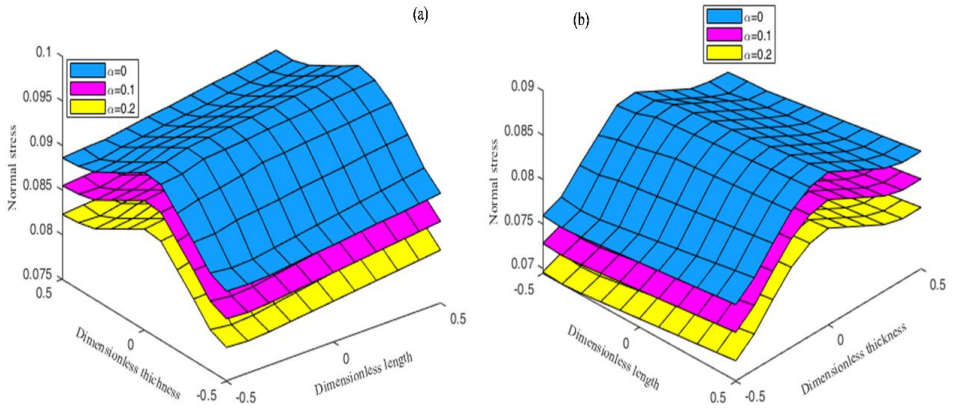

Figure. 14. Variation in normal stress $\overline{\sigma}_{z}$ values of CC beam with even (a) and uneven (b) porosity, aspect ratio (L/h = 5), and gradation exponents

CF beams, for various aspect ratios and gradation exponents, are tested with UDL to estimate transverse deflection, axial stress, shear stress, and normal stress. As the aspect ratio increases, dimensionless transverse deflection reduces, whereas dimensionless transverse deflection increases with gradation exponents [65, 69]. As demonstrated in Figure 15, transverse deflection increases as the porosity index and gradation exponents increase. The transverse deflection value in even porosity distribution is greater than that in uneven porosity distribution [66, 70]. The axial stress decreases along with the beam's thickness from the bottom to top, with the highest axial stress occurring at a gradation exponent of 10. Refer to Figure 16. Shear stress is zero at the top and bottom of the beam, and its greatest value is at gradation exponent level 2, as seen in Figure 17. Maximum normal stress occurred at the top of the beam, as presented in Figure 18.

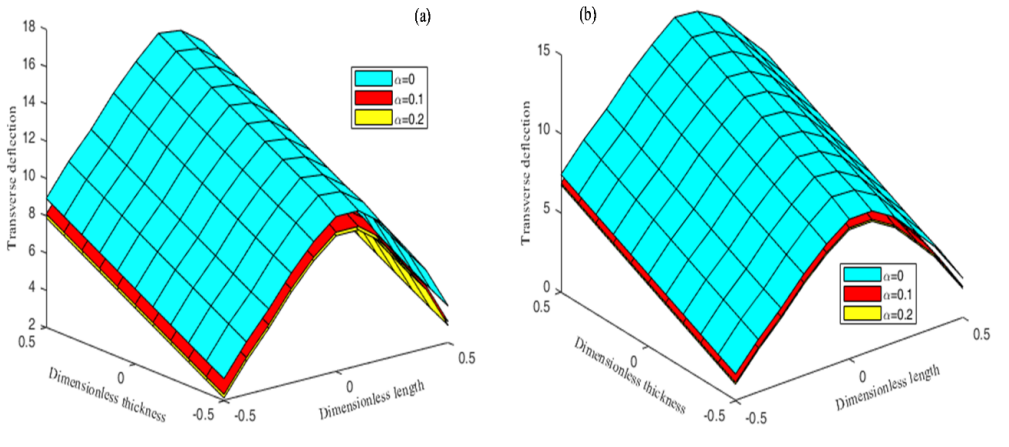

Figure. 15. Variation in transverse deflections $\overline{w}$ values of CF beam with even (a) and uneven (b) porosity, aspect ratio (L/h = 5), and gradation exponents

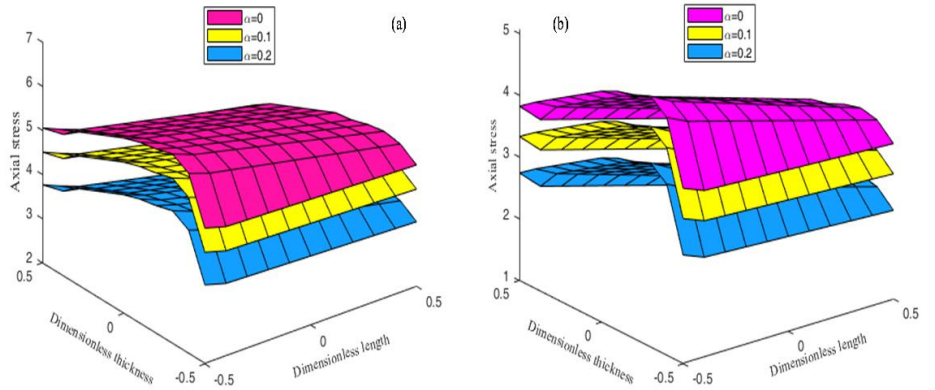

Figure. 16. Variation in axial stress $\overline{\sigma}_x$ values of CF beam with even and uneven porosity, aspect ratio (L/h = 5), and gradation exponents

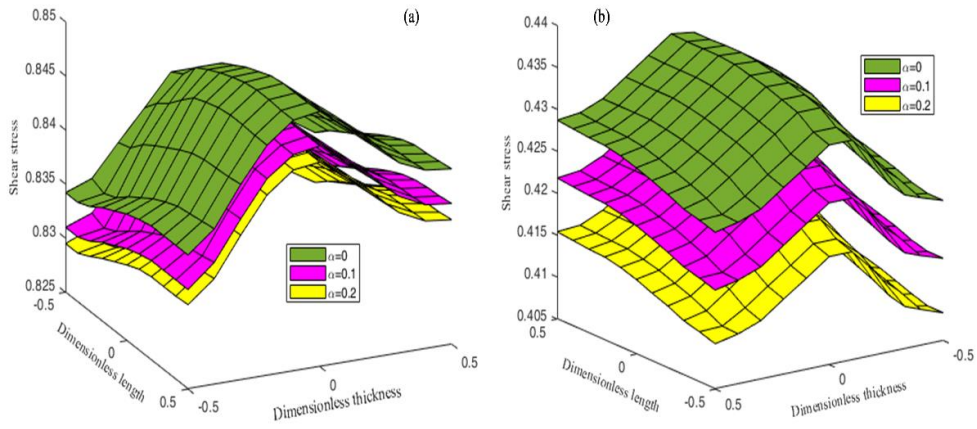

Figure. 17. Variation in shear stress $\overline{\sigma}_{xz}$ values of CF beam with even (a) and uneven (b) porosity, aspect ratio (L/h = 5), and gradation exponents

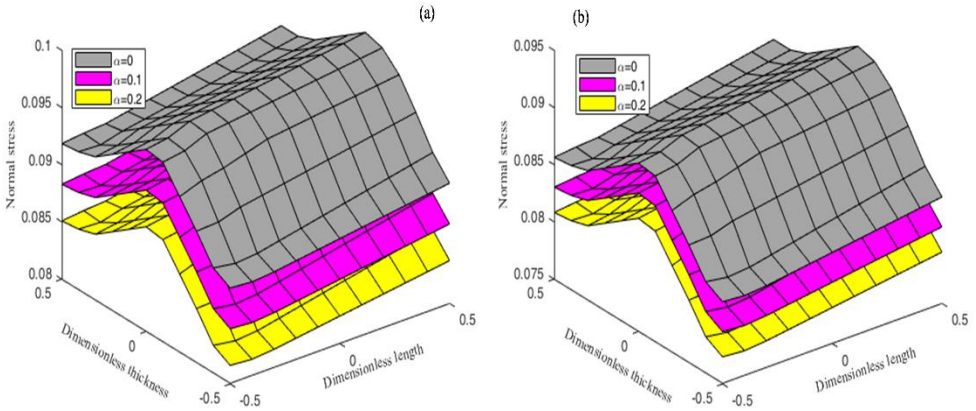

Figure. 18. Variation in normal stress $\overline{\sigma}_z$ values of CF beam with even (a) and uneven (b) porosity, aspect ratio (L/h = 5), and gradation exponents

4. Conclusion

HSDT is applied in order to conduct an analysis of the elastostatic behaviour of 2D-FGPB that is subjected to various boundary conditions and a load that is uniformly distributed. An evaluation of transverse deflections, axial, normal, and shear stresses is carried out. The developed method is checked for accuracy by analysing a 2D-FGPB with simply supported and comparing the results with those of earlier research and analytical solutions. There are three distinct boundary conditions that are taken into consideration: SS, CC, and CF. Noteworthy findings of the analysis are listed below:

- The boundary conditions each have a unique influence on gradation exponents in length and thickness directions and in aspect ratios.
- An increase in the power law index will result in a reduction in the stiffness of the 2D-FGPB, resulting in increase in the deflections.
- The transverse deflection, axial stress, shear stress, and normal stress of the 2D-FGPB are significantly influenced by the gradient indexes in a substantial way. On the other hand, the influence of the gradient index in x direction is significant than its influence in the z direction.
- The porosity parameter is an important thing to think about when building modern structures, and the amount of porosity in a structure can have a big effect.

Based on the results of the three numerical examples presented above, it can be concluded that the HSDT can be used for analysis in linear, two-directional, functionally graded porous beams. Accurate analysis could be done by using HSDT and could be applied to thick beams only. The effect on normal strain can be investigated further.

Nomenclature

2D- FGPB	Two- directional functionally graded porous beam
CBT	Classical beam theory
CC	Clamped-clamped
CF	Clamped free
E	Modulus of elasticity [GPa]
FG	Functionally graded
FGB	Functionally graded beam
FGM	Functionally graded material
f(z)	Shear shape function
h	Height [m]
HSDT	Higher order shear deformation theory
K	Shear correction factor
L	Length [m]

UDL	Uniformly distributed load
p_x	Gradient index in the length direction
p_z	Gradient index in the thickness direction
SS	Simply supported
V_f	Volume fraction
x,y, z	Different coordinates along length, width, and thickness directions of beam
α	Coefficient of porosity/ Porosity index
μ	Poisson's ratio
ρ	Mass density[Kg/m^3]
δU	Strain energy
δk	Kinetic energy
ϕ	Shear slope
$\frac{\partial w_0}{\partial x}$	Bending slope

References

[1] Y. Miyamoto, W. Kaysser, B. Rabin, A. Kawasaki, R. G. Ford, Processing and fabrication, *Functionally Graded Materials: Design, Processing and Applications*, pp. 161-245, 1999.

[2] M. Mohammadi, A. Farajpour, A. Moradi, M. Hosseini, Vibration analysis of the rotating multilayer piezoelectric Timoshenko nanobeam, *Engineering Analysis with Boundary Elements,* Vol. 145, pp. 117-131, 2022.

[3] M. Mohammadi, A. Rastgoo, Primary and secondary resonance analysis of FG/lipid nanoplate with considering porosity distribution based on a nonlinear elastic medium, *Mechanics of Advanced Materials and Structures,* Vol. 27, No. 20, pp. 1709-1730, 2020.

[4] M. Mohammadi, M. Hosseini, M. Shishesaz, A. Hadi, A. Rastgoo, Primary and secondary resonance analysis of porous functionally graded nanobeam resting on a nonlinear foundation subjected to mechanical and electrical loads, *European Journal of Mechanics-A/Solids,* Vol. 77, pp. 103793, 2019.

[5] M. Mohammadi, A. Rastgoo, Nonlinear vibration analysis of the viscoelastic composite nanoplate with three directionally imperfect porous FG core, *Structural Engineering and Mechanics, An Int'l Journal,* Vol. 69, No. 2, pp. 131-143, 2019.

[6] A. Farajpour, A. Rastgoo, M. Mohammadi, Vibration, buckling and smart control of microtubules using piezoelectric nanoshells under electric voltage in thermal environment, *Physica B: Condensed Matter,* Vol. 509, pp. 100-114, 2017.

[7] A. Farajpour, M. H. Yazdi, A. Rastgoo, M. Loghmani, M. Mohammadi, Nonlocal nonlinear plate model for large amplitude vibration of magneto-electro-elastic nanoplates, *Composite Structures,* Vol. 140, pp. 323-336, 2016.

[8] A. Farajpour, M. H. Yazdi, A. Rastgoo, M. Mohammadi, A higher-order nonlocal strain gradient plate model for buckling of orthotropic nanoplates in thermal environment, *Acta Mechanica,* Vol. 227, pp. 1849-1867, 2016.

[9] M. Mohammadi, M. Safarabadi, A. Rastgoo, A. Farajpour, Hygro-mechanical vibration analysis of a rotating viscoelastic nanobeam embedded in a visco-Pasternak elastic medium and in a nonlinear thermal environment, *Acta Mechanica,* Vol. 227, pp. 2207-2232, 2016.

[10] M. R. Farajpour, A. Rastgoo, A. Farajpour, M. Mohammadi, Vibration of piezoelectric nanofilm-based electromechanical sensors via higher-order non-local strain gradient theory, *Micro & Nano Letters,* Vol. 11, No. 6, pp. 302-307, 2016.

[11] M. Baghani, M. Mohammadi, A. Farajpour, Dynamic and stability analysis of the rotating nanobeam in a nonuniform magnetic field considering the surface energy, *International Journal of Applied Mechanics,* Vol. 8, No. 04, pp. 1650048, 2016.

[12] M. Goodarzi, M. Mohammadi, M. Khooran, F. Saadi, Thermo-mechanical vibration analysis of FG circular and annular nanoplate based on the visco-pasternak foundation, *Journal of Solid Mechanics,* Vol. 8, No. 4, pp. 788-805, 2016.

[13] H. Asemi, S. Asemi, A. Farajpour, M. Mohammadi, Nanoscale mass detection based on vibrating piezoelectric ultrathin films under thermo-electro-mechanical loads, *Physica E: Low-dimensional Systems and Nanostructures*, Vol. 68, pp. 112-122, 2015.

[14] M. Safarabadi, M. Mohammadi, A. Farajpour, M. Goodarzi, Effect of surface energy on the vibration analysis of rotating nanobeam, 2015.

[15] M. Goodarzi, M. Mohammadi, A. Gharib, Techno-Economic Analysis of Solar Energy for Cathodic Protection of Oil and Gas Buried Pipelines in Southwestern of Iran, in *Proceeding of*, https://publications.waset.org/abstracts/33008/techno-economic-analysis-of …, pp.

[16] M. Mohammadi, A. A. Nekounam, M. Amiri, The vibration analysis of the composite natural gas pipelines in the nonlinear thermal and humidity environment, in *Proceeding of*, https://civilica.com/doc/540946/, pp.

[17] M. Goodarzi, M. Mohammadi, M. Rezaee, Technical Feasibility Analysis of PV Water Pumping System in Khuzestan Province-Iran, in *Proceeding of*, https://publications.waset.org/abstracts/18930/technical-feasibility …, pp.

[18] M. Mohammadi, A. Farajpour, A. Moradi, M. Ghayour, Shear buckling of orthotropic rectangular graphene sheet embedded in an elastic medium in thermal environment, *Composites Part B: Engineering*, Vol. 56, pp. 629-637, 2014.

[19] M. Mohammadi, A. Moradi, M. Ghayour, A. Farajpour, Exact solution for thermo-mechanical vibration of orthotropic mono-layer graphene sheet embedded in an elastic medium, *Latin American Journal of Solids and Structures*, Vol. 11, pp. 437-458, 2014.

[20] M. Mohammadi, A. Farajpour, M. Goodarzi, F. Dinari, Thermo-mechanical vibration analysis of annular and circular graphene sheet embedded in an elastic medium, *Latin American Journal of Solids and Structures*, Vol. 11, pp. 659-682, 2014.

[21] M. Mohammadi, A. Farajpour, M. Goodarzi, Numerical study of the effect of shear in-plane load on the vibration analysis of graphene sheet embedded in an elastic medium, *Computational Materials Science*, Vol. 82, pp. 510-520, 2014.

[22] A. Farajpour, A. Rastgoo, M. Mohammadi, Surface effects on the mechanical characteristics of microtubule networks in living cells, *Mechanics Research Communications*, Vol. 57, pp. 18-26, 2014.

[23] S. R. Asemi, M. Mohammadi, A. Farajpour, A study on the nonlinear stability of orthotropic single-layered graphene sheet based on nonlocal elasticity theory, *Latin American Journal of Solids and Structures*, Vol. 11, pp. 1541-1546, 2014.

[24] M. Goodarzi, M. Mohammadi, A. Farajpour, M. Khooran, Investigation of the effect of pre-stressed on vibration frequency of rectangular nanoplate based on a visco-Pasternak foundation, 2014.

[25] S. Asemi, A. Farajpour, H. Asemi, M. Mohammadi, Influence of initial stress on the vibration of double-piezoelectric-nanoplate systems with various boundary conditions using DQM, *Physica E: Low-dimensional Systems and Nanostructures*, Vol. 63, pp. 169-179, 2014.

[26] S. Asemi, A. Farajpour, M. Mohammadi, Nonlinear vibration analysis of piezoelectric nanoelectromechanical resonators based on nonlocal elasticity theory, *Composite Structures*, Vol. 116, pp. 703-712, 2014.

[27] M. Mohammadi, M. Ghayour, A. Farajpour, Free transverse vibration analysis of circular and annular graphene sheets with various boundary conditions using the nonlocal continuum plate model, *Composites Part B: Engineering*, Vol. 45, No. 1, pp. 32-42, 2013.

[28] M. Mohammadi, M. Goodarzi, M. Ghayour, A. Farajpour, Influence of in-plane pre-load on the vibration frequency of circular graphene sheet via nonlocal continuum theory, *Composites Part B: Engineering*, Vol. 51, pp. 121-129, 2013.

[29] M. Mohammadi, A. Farajpour, M. Goodarzi, R. Heydarshenas, Levy type solution for nonlocal thermo-mechanical vibration of orthotropic mono-layer graphene sheet embedded in an elastic medium, *Journal of Solid Mechanics*, Vol. 5, No. 2, pp. 116-132, 2013.

[30] M. Mohammadi, A. Farajpour, M. Goodarzi, H. Mohammadi, Temperature Effect on Vibration Analysis of Annular Graphene Sheet Embedded on Visco-Pasternak Foundati, *Journal of Solid Mechanics*, Vol. 5, No. 3, pp. 305-323, 2013.

[31] M. Danesh, A. Farajpour, M. Mohammadi, Axial vibration analysis of a tapered nanorod based on nonlocal elasticity theory and differential quadrature method, *Mechanics Research Communications*, Vol. 39, No. 1, pp. 23-27, 2012.

[32] A. Farajpour, A. Shahidi, M. Mohammadi, M. Mahzoon, Buckling of orthotropic micro/nanoscale plates under linearly varying in-plane load via nonlocal continuum mechanics, *Composite Structures*, Vol. 94, No. 5, pp. 1605-1615, 2012.

[33] M. Mohammadi, M. Goodarzi, M. Ghayour, S. Alivand, Small scale effect on the vibration of orthotropic plates embedded in an elastic medium and under biaxial in-plane pre-load via nonlocal elasticity theory, 2012.

[34] A. Farajpour, M. Mohammadi, A. Shahidi, M. Mahzoon, Axisymmetric buckling of the circular graphene sheets with the nonlocal continuum plate model, *Physica E: Low-dimensional Systems and Nanostructures,* Vol. 43, No. 10, pp. 1820-1825, 2011.

[35] A. Farajpour, M. Danesh, M. Mohammadi, Buckling analysis of variable thickness nanoplates using nonlocal continuum mechanics, *Physica E: Low-dimensional Systems and Nanostructures,* Vol. 44, No. 3, pp. 719-727, 2011.

[36] H. Moosavi, M. Mohammadi, A. Farajpour, S. Shahidi, Vibration analysis of nanorings using nonlocal continuum mechanics and shear deformable ring theory, *Physica E: Low-dimensional Systems and Nanostructures,* Vol. 44, No. 1, pp. 135-140, 2011.

[37] M. Mohammadi, M. Ghayour, A. Farajpour, Analysis of free vibration sector plate based on elastic medium by using new version differential quadrature method, *Journal of solid mechanics in engineering,* Vol. 3, No. 2, pp. 47-56, 2011.

[38] A. Farajpour, M. Mohammadi, M. Ghayour, Shear buckling of rectangular nanoplates embedded in elastic medium based on nonlocal elasticity theory, in *Proceeding of,* www.civilica.com/Paper-ISME19-ISME19_390.html, pp. 390.

[39] M. Mohammadi, A. Farajpour, A. R. Shahidi, Higher order shear deformation theory for the buckling of orthotropic rectangular nanoplates using nonlocal elasticity, in *Proceeding of,* www.civilica.com/Paper-ISME19-ISME19_391.html, pp. 391.

[40] M. Mohammadi, A. Farajpour, A. R. Shahidi, Effects of boundary conditions on the buckling of single-layered graphene sheets based on nonlocal elasticity, in *Proceeding of,* www.civilica.com/Paper-ISME19-ISME19_382.html, pp. 382.

[41] M. Mohammadi, M. Ghayour, A. Farajpour, Using of new version integral differential method to analysis of free vibration orthotropic sector plate based on elastic medium, in *Proceeding of,* www.civilica.com/Paper-ISME19-ISME19_497.html, pp. 497.

[42] M. Mohammadi, A. Farajpour, A. Rastgoo, Coriolis effects on the thermo-mechanical vibration analysis of the rotating multilayer piezoelectric nanobeam, *Acta Mechanica,* Vol. 234, No. 2, pp. 751-774, 2023/02/01, 2023.

[43] J. Kim, K. K. Żur, J. Reddy, Bending, free vibration, and buckling of modified couples stress-based functionally graded porous micro-plates, *Composite Structures,* Vol. 209, pp. 879-888, 2019.

[44] J. Parthasarathy, B. Starly, S. Raman, A design for the additive manufacture of functionally graded porous structures with tailored mechanical properties for biomedical applications, *Journal of Manufacturing Processes,* Vol. 13, No. 2, pp. 160-170, 2011.

[45] M. Babaei, F. Kiarasi, K. Asemi, M. Hosseini, Functionally graded saturated porous structures: A review, *Journal of Computational Applied Mechanics,* Vol. 53, No. 2, pp. 297-308, 2022.

[46] N.-D. Nguyen, T.-N. Nguyen, T.-K. Nguyen, T. P. Vo, A new two-variable shear deformation theory for bending, free vibration and buckling analysis of functionally graded porous beams, *Composite Structures,* Vol. 282, pp. 115095, 2022.

[47] N. Wattanasakulpong, B. G. Prusty, D. W. Kelly, Thermal buckling and elastic vibration of third-order shear deformable functionally graded beams, *International Journal of Mechanical Sciences,* Vol. 53, No. 9, pp. 734-743, 2011.

[48] A. Melaibari, R. M. Abo-bakr, S. Mohamed, M. Eltaher, Static stability of higher order functionally graded beam under variable axial load, *Alexandria Engineering Journal,* Vol. 59, No. 3, pp. 1661-1675, 2020.

[49] D. Chen, S. Kitipornchai, J. Yang, Nonlinear free vibration of shear deformable sandwich beam with a functionally graded porous core, *Thin-Walled Structures,* Vol. 107, pp. 39-48, 2016.

[50] D. Chen, J. Yang, S. Kitipornchai, Free and forced vibrations of shear deformable functionally graded porous beams, *International journal of mechanical sciences,* Vol. 108, pp. 14-22, 2016.

[51] D. Wu, A. Liu, Y. Huang, Y. Huang, Y. Pi, W. Gao, Dynamic analysis of functionally graded porous structures through finite element analysis, *Engineering Structures,* Vol. 165, pp. 287-301, 2018.

[52] K. Gao, R. Li, J. Yang, Dynamic characteristics of functionally graded porous beams with interval material properties, *Engineering Structures,* Vol. 197, pp. 109441, 2019.

[53] A. R. Noori, T. A. Aslan, B. Temel, Dynamic analysis of functionally graded porous beams using complementary functions method in the Laplace domain, *Composite Structures,* Vol. 256, pp. 113094, 2021.

[54] Z. Lei, L. Zhang, K. Liew, J. Yu, Dynamic stability analysis of carbon nanotube-reinforced functionally graded cylindrical panels using the element-free kp-Ritz method, *Composite Structures,* Vol. 113, pp. 328-338, 2014.

[55] M. Filippi, M. Petrolo, S. Valvano, E. Carrera, Analysis of laminated composites and sandwich structures by trigonometric, exponential and miscellaneous polynomials and a MITC9 plate element, *Composite Structures,* Vol. 150, pp. 103-114, 2016.

[56] F. A. Fazzolari, Generalized exponential, polynomial and trigonometric theories for vibration and stability analysis of porous FG sandwich beams resting on elastic foundations, *Composites Part B: Engineering,* Vol. 136, pp. 254-271, 2018.

[57] O. Polit, C. Anant, B. Anirudh, M. Ganapathi, Functionally graded graphene reinforced porous nanocomposite curved beams: Bending and elastic stability using a higher-order model with thickness stretch effect, *Composites Part B: Engineering,* Vol. 166, pp. 310-327, 2019.

[58] R. Shimpi, P. Guruprasad, K. Pakhare, Simple two variable refined theory for shear deformable isotropic rectangular beams, *Journal of Applied and Computational Mechanics,* Vol. 6, No. 3, pp. 394-415, 2020.

[59] A. Assie, S. D. Akbas, A. M. Kabeel, A. A. Abdelrahman, M. A. Eltaher, Dynamic analysis of porous functionally graded layered deep beams with viscoelastic core, *STEEL AND COMPOSITE STRUCTURES,* Vol. 43, No. 1, pp. 79-90, 2022.

[60] B. Anirudh, M. Ganapathi, C. Anant, O. Polit, A comprehensive analysis of porous graphene-reinforced curved beams by finite element approach using higher-order structural theory: Bending, vibration and buckling, *Composite Structures,* Vol. 222, pp. 110899, 2019.

[61] W. Fang, T. Yu, T. Q. Bui, Analysis of thick porous beams by a quasi-3D theory and isogeometric analysis, *Composite Structures,* Vol. 221, pp. 110890, 2019.

[62] F. Ebrahimi, N. Farazmandnia, Vibration analysis of functionally graded carbon nanotube-reinforced composite sandwich beams in thermal environment, *Advances in aircraft and spacecraft science,* Vol. 5, No. 1, pp. 107, 2018.

[63] Y. S. Al Rjoub, A. G. Hamad, Free Vibration of Axially Loaded Multi-Cracked Beams Using the Transfer Matrix Method, *International Journal of Acoustics & Vibration,* Vol. 24, No. 1, 2019.

[64] J. Zhao, Q. Wang, X. Deng, K. Choe, R. Zhong, C. Shuai, Free vibrations of functionally graded porous rectangular plate with uniform elastic boundary conditions, *Composites Part B: Engineering,* Vol. 168, pp. 106-120, 2019.

[65] M. Jamshidi, J. Arghavani, Optimal material tailoring of functionally graded porous beams for buckling and free vibration behaviors, *Mechanics Research Communications,* Vol. 88, pp. 19-24, 2018.

[66] V. K. Nathi, Buckling analysis of 2D functionally graded porous beams using novel higher order theory, *Journal of Computational Applied Mechanics,* Vol. 53, No. 3, pp. 393-413, 2022.

[67] A. Karamanlı, Free vibration analysis of two directional functionally graded beams using a third order shear deformation theory, *Composite Structures,* Vol. 189, pp. 127-136, 2018.

[68] T. P. Vo, H.-T. Thai, T.-K. Nguyen, F. Inam, J. Lee, Static behaviour of functionally graded sandwich beams using a quasi-3D theory, *Composites Part B: Engineering,* Vol. 68, pp. 59-74, 2015.

[69] A. Karamanlı, Bending analysis of two directional functionally graded beams using a four-unknown shear and normal deformation theory, *Politeknik Dergisi,* Vol. 21, No. 4, pp. 861-874, 2018.

[70] G. Reddy, N. V. Kumar, Bending Analysis of 2-D Functionally Graded Porous Beams Based on Novel High Order Theory, *Journal of Engineering Science & Technology Review,* Vol. 15, No. 5, 2022.